Shahid Bahonar University of Kerman

Biomechanism and Bioenergy Research

Online ISSN: 2821-1855
Homepage: https://bbr.uk.ac.ir

Iranian Society of Agricultural Machinery Engineering and Mechanization

A Comprehensive Machine Learning Framework for Detection of Red Sumac (Rhus coriaria) Adulteration with Barberry Using Hyperspectral Imaging

Seyedehsamaneh Shojaeilangari[1], Esmat Kishani Farahani[2], Farahnaz Rahmani[1] Alireza Bassiri[3]

[1] Biomedical Engineering Group, Department of Electrical Engineering and Information Technology, Iranian Research Organization for Science and Technology (IROST), 33535111, Tehran, Iran
[2] Information Technology and Intelligent Systems Group, Department of Electrical Engineering and Information Technology, Iranian Research Organization for Science and Technology (IROST), 33535111, Tehran, Iran
[3] Department of Chemical Technologies, Iranian Research Organization for Science and Technology (IROST), 33535111, Tehran, Iran

Corresponding author: s.shojaie@irost.ir

ARTICLE INFO

Article type:

Research Article

Article history:

Received 11 March 2026

Received in revised form 08 April 2026

Accepted 01 May 2026

Available Online 30 June 2026

Keywords:

Hyperspectral imaging, Sumac adulteration, Machine learning, Feature extraction, Deep learning.

ABSTRACT

This research proposes a comprehensive machine learning framework for detecting red sumac adulteration with barberry using hyperspectral imaging. Various features including statistical features, Discrete Cosine Transform (DCT) features, and shape features were extracted and analyzed for classification performance. Results demonstrate that among traditional classifiers, Random Forest achieved the highest accuracy (91.11%) when utilizing all features, with statistical features having the most significant impact on classification. Among deep learning approaches, LSTM networks outperformed all other methods with accuracy exceeding 96%, demonstrating the importance of sequential spectral information in adulteration detection. Further analysis revealed that even with aggressive spectral down sampling (30×), the LSTM model maintained high accuracy (93.9%), suggesting potential for implementation in cost-effective systems. These findings advance food authentication technology by offering both high-performance detection methods and practical implementation strategies for identifying red sumac adulteration, contributing to food safety and quality assurance efforts.

Cite this article: Shojaeilangari, S., Kishani Farahani, E., Rahmani, F., & Bassiri, A. (2026). A Comprehensive Machine Learning Framework for Detection of Red Sumac (Rhus coriaria) Adulteration with Barberry Using Hyperspectral Imaging. *Biomechanism and Bioenergy Research*, *5*(2), 84-11. https://doi.org/10.22103/bbr.2026.27386.1157

Publisher: Shahid Bahonar University of Kerman
DOI: https://doi.org/10.22103/bbr.2026.27386.1157

INTRODUCTION

Sumac (*Rhus coriaria*) is a prominent spice in Middle Eastern, Mediterranean, and Western Asian cuisines, valued for its sour taste, vibrant red color, and antioxidant properties (Grivetti, 2016). Derived from the dried fruits of the sumac plant, it is used both as a flavoring agent and in traditional medicine. The growing global demand for spices has, however, led to an increase in the market price of sumac, making it a target for economically motivated adulteration (Galvin-King et al., 2018).

Adulteration of sumac often involves the addition of cheaper materials such as barberry powder (*Berberis vulgaris*), pomegranate peels, artificial colorants, or other plant substances. Such fraudulent practices not only diminish the economic value and quality of the product but can also pose potential health risks to consumers (Johnson et al., 2025). Traditional methods for detecting adulteration, which rely on sensory evaluation (e.g., taste, smell, color) and basic chemical tests, are often subjective, time-consuming, and lack the precision to detect sophisticated adulterations, particularly at low contamination levels (Sahu et al., 2023; Sharma & MMR, 2022). While advanced analytical techniques like high-performance liquid chromatography (HPLC) and gas chromatography (GC) offer greater accuracy, they are typically destructive, expensive, and require specialized personnel, limiting their use for routine screening (Johnson et al., 2025; Sebaei et al., 2019).

In response to these limitations, rapid, non-destructive analytical techniques have gained significant attention for food authentication. Hyperspectral imaging (HSI) is one such innovative method that integrates conventional imaging with spectroscopy to simultaneously capture spatial and spectral information from a sample (Fu et al., 2022; Meng et al., 2020). HSI generates a data cube containing the reflectance or absorbance spectrum for each pixel, revealing subtle differences in the physical and chemical composition of materials. When combined with machine learning, HSI has proven to be a powerful tool for detecting adulteration in various spices. For instance, Khan et al. used HSI to detect color adulteration in red chili powder with 100% accuracy using a support vector machine (SVM) classifier (Khan et al., 2020). Similarly, Orrillo et al. employed near-infrared HSI to identify papaya seed adulteration in black pepper, while Kiani et al. authenticated nutmeg powder and detected spent material adulteration using a handheld HSI system and artificial neural networks (ANN) (Kiani et al., 2019; Orrillo et al., 2019). Furthermore, Schumer et al. developed a multi-spice calibration model using NIR spectroscopy to detect low levels (1-10%) of corn starch adulteration in six different organic spices (Schumer et al., 2025).

The detection of barberry adulteration in red sumac is particularly challenging due to the similarities in color and texture between the two materials, necessitating highly sensitive and precise methods. Traditional adulteration detection techniques—such as HPLC, PCR, and visual inspection—are time-consuming, destructive, require skilled personnel, and are impractical for rapid, non-destructive screening of large sample volumes. In contrast, HSI combined with machine learning offers a rapid, non-destructive, and high-throughput alternative (Ferrari et al., 2024; Kishani Farahani & Shojaielangari, 2026; Shojaeilangari et al., 2026). Deep learning approaches have shown exceptional performance in hyperspectral image classification across numerous domains (Ahmad et al., 2021; Signoroni et al., 2019), but their application to food adulteration detection, especially for spices like sumac, has not been fully explored. Existing studies predominantly rely on convolutional architectures as well as the practical constraints of real-world deployment (Liu et al., 2025). Furthermore, prior work on sumac has focused on brown sumac rather than red sumac adulteration with barberry (Kishani Farahani & Shojaielangari, 2026), leaving a clear gap in the literature. To address this gap, this study develops a comprehensive machine learning framework that integrates HSI with both

traditional feature engineering and modern deep learning architectures to authenticate red sumac and detect barberry adulteration.

To our knowledge, this work presents the first systematic comparison of traditional machine learning and deep learning approaches for this specific adulteration scenario, yielding three key methodological advances: (1) Long Short-Term Memory (LSTM) networks significantly outperform CNN-based and traditional models by effectively capturing sequential spectral dependencies; (2) statistical spectral features dominate classification performance over Discrete Cosine Transform (DCT) or shape-based descriptors; and (3) aggressive spectral downsampling (30×) maintains >93.9% accuracy, demonstrating a viable pathway for cost-effective, field-deployable authentication systems.

The principal contributions of this work are fourfold:

- Development of a robust, multi-modal feature set combining statistical, shape, and transform-based descriptors extracted from hyperspectral data.
- Comprehensive benchmarking of traditional classifiers (Random Forest, Gradient Boosting, SVM, and K-Nearest Neighbors) against deep learning architectures (CNN, LSTM, and hybrid CNN-LSTM) under unified experimental conditions.
- Demonstration of high-sensitivity adulteration detection at concentrations as low as 5%, highlighting the framework's ability to resolve subtle spectral differences.
- Identification of critical diagnostic spectral regions (particularly 680–700 nm), providing actionable insights for the development of simplified, multispectral screening devices.

This research advances rapid, non-destructive food authentication by offering both high-performance detection methodologies and practical implementation strategies. The proposed framework is readily adaptable to other spice adulteration scenarios, supporting broader food safety and quality assurance efforts.

MATERIALS AND METHODS

An overview of the experimental workflow is illustrated in Figure 1. As shown in the figure, the proposed methodology comprises five main steps, each of which is described in detail in the following subsections: sample preparation**,** HSI acquisition**,** spectral preprocessing**,** feature extraction**,** and classification using traditional machine learning and deep learning methods.

Indeed, this study develops a comprehensive machine learning framework that integrates HSI with both traditional feature engineering and modern deep learning architectures—including CNN, LSTM networks, and a hybrid CNN-LSTM model—to authenticate red sumac (*Rhus coriaria*) and detect barberry (*Berberis vulgaris*) adulteration. The framework was rigorously evaluated using pure sumac samples and those adulterated with barberry at six concentration levels: 0% (pure sumac), 5%, 20%, 35%, 50%, and 100% (pure barberry).

The proposed framework is readily adaptable to other spice adulteration scenarios, supporting broader food safety and quality assurance efforts.

.

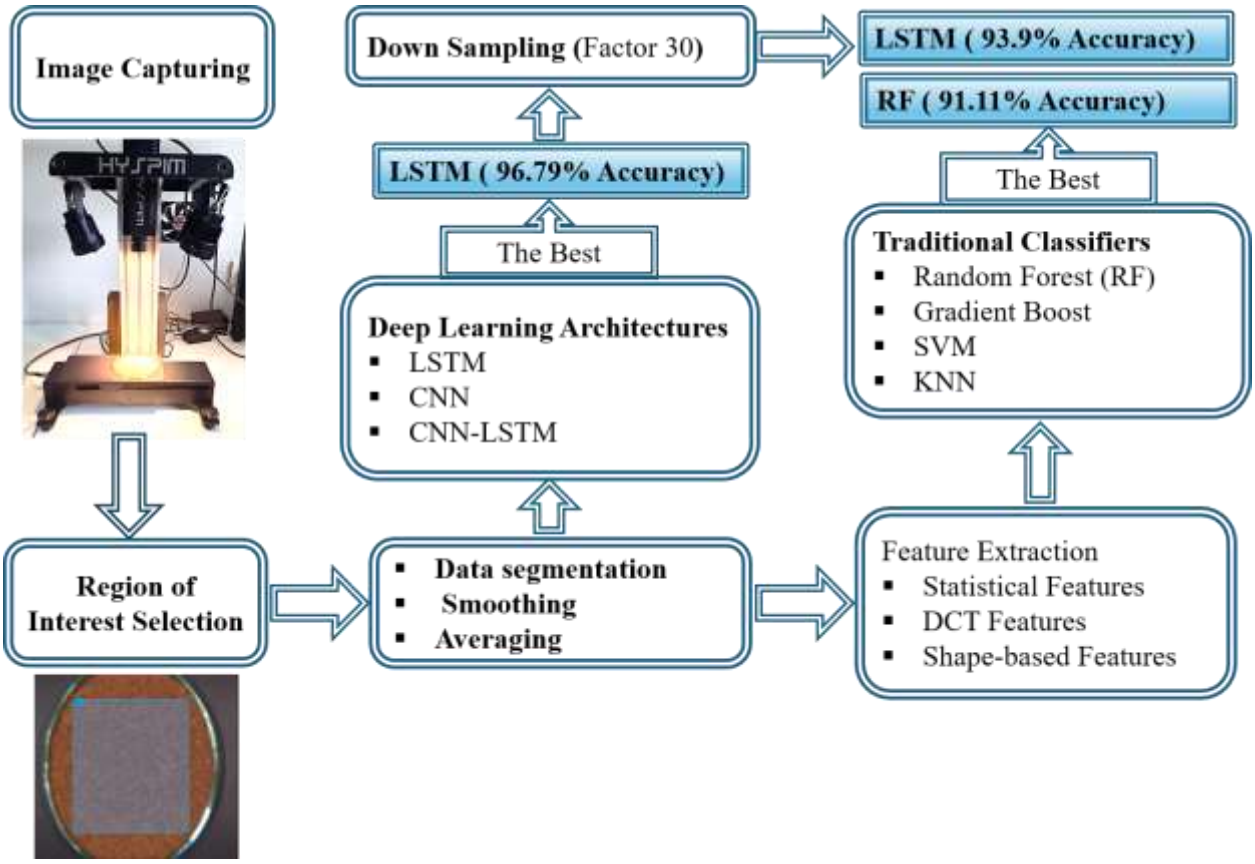

Figure 1. Overview of the research workflow for detection of red Sumac adulteration with barberry using hyperspectral imaging and a comprehensive machine learning framework.

Sample Preparation Method

To prepare the samples, authentic red sumac seeds were first purchased from a reliable supplier (Figure 2a). The seeds were cleaned and all foreign matter was removed. Then, the samples were dried in a convection oven at 40°C until reaching an average final moisture content of 8% on a wet basis. The dried samples were ground with an electric grinder (IKA, model A11, Germany) and passed through a 35-mesh sieve. The obtained powders were placed in glass jars and stored away from light and at 4°C.

Additionally, barberry fruits with a color similar to red sumac were obtained from the market (Figure 2b). These fruits were pressed to extract the juice, after which the remaining pomace was dried, ground, and sieved to achieve the same maximum particle diameter as the sumac samples.

Adulterated samples were then prepared by mixing the ground barberry pomace with the pure ground sumac at mass percentages of 0%, 5%, 20%, 35%, and 50%. For each mixture, 10 grams were placed in an 8 cm diameter Petri dish. Five replicate Petri dishes were prepared for each adulteration level (Figure 2c).

a) b) c)

Figure 2. a) Red sumac seeds. b) Ground red sumac and barberry with suitable color similarity. c) Prepared sumac samples. Each column represents the replicates for one mixture. From right to left, the columns correspond to samples with adulteration levels of 0%, 5%, 20%, 35%, 50%, and 100% respectively.

Hyperspectral Image Acquisition

Hyperspectral images were acquired using a benchtop line-scanning (push-broom) system (Parto Afzar Sannat Company, Tehran, Iran). The system operates over a visible to near-infrared wavelength range (400-950 nm) with 993 spectral channels**.** The spatial resolution is 210 µm**.** light sources of the system (three 50 W halogen lamps) are positioned at a 45° angle relative to the sample surface. The camera is mounted at a fixed distance of 30 cm above the sample stage.

At the beginning of the measurements, the light sources were turned on and allowed to stabilize for 2.5 minutes to achieve consistent illumination intensity. The system was then calibrated using white and dark references**.** The scan length was set to 110 mm, and each sample was placed in a Petri dish. A hyperspectral image was then captured for each Petri dish (Figure 3).

.

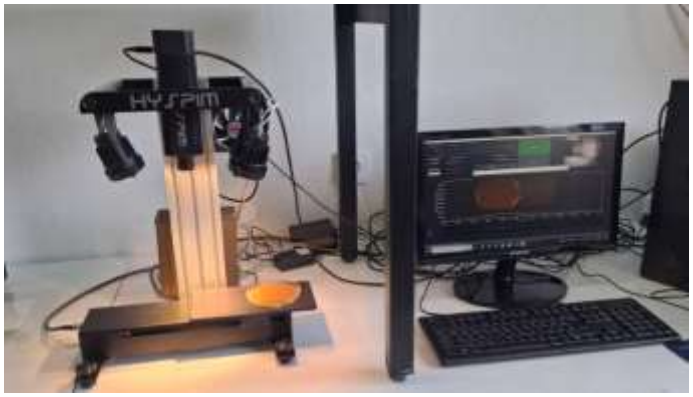

Figure 3. Hyperspectral imaging system.

Data Preprocessing

Data preprocessing involved spatial and spectral steps. Spatially, region of interest in each hyperspectral image was subdivided into non-overlapping 10×10 pixel segments to enhance dataset, producing 30 segments per image (Figure 4a). With five images per sample and five samples per concentration level, this resulted in 150 segments for each specific impurity percentage. Spectrally, a Savitzky-Golay smoothing filter (Savitzky & Golay, 1964) (polynomial order: 3, window length: 7) was applied to each 3D image segment to suppress noise. Indeed, Savitzky-Golay filter, which applies a local polynomial regression to each spectral window to smooth noise while preserving high-frequency spectral features. Unlike simple moving averages, the Savitzky-Golay filter maintains the shape and width of spectral peaks by fitting a low-degree polynomial

to a sliding window of 7 neighboring wavelength bands. The smoothed value at each band is obtained from the polynomial's central point. This method is particularly effective for hyperspectral data because it reduces random noise from the detector and environmental fluctuations without distorting absorption features critical for adulteration detection.

The mean reflectance spectrum of all pixels within a segment was then computed to serve as its representative spectral signature. Consequently, a comprehensive dataset of 900 samples was established, spanning six concentration levels (0%, 5%, 20%, 35%, 50%, and 100%) and characterized by 993 spectral features each. Mean reflectance spectra of six concentration levels are illustrated in Figure 4b.

.

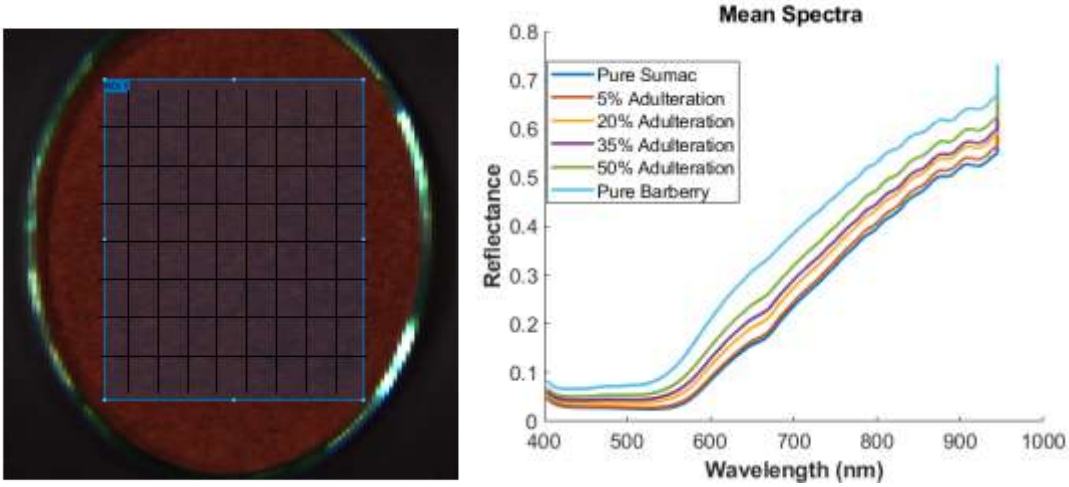

a) b)

Figure 4. a) Spatial subdivision of the region of interest into 10×10 pixel non-overlapping segments to increase dataset size. b) Mean reflectance spectra of six concentration levels.

Feature Extraction

A three-tiered approach including statistical, DCT, and shape features were employed to comprehensively characterize spectral differences between pure and adulterated sumac samples. First, advanced statistical features provided fundamental quantitative descriptors including central tendency measures (mean, median), dispersion metrics (standard deviation, range, interquartile range), and distribution shape characteristics (skewness, kurtosis). These features were complemented by derivative-based features (first derivative as slope representation and second derivative as curvature representation), particularly within the 650-750nm region where subtle spectral variations manifested. The statistical suite also included specialized metrics like slope ratios comparing spectral behavior before and after the critical region, offering robust discrimination capabilities across the adulteration gradient.

Second, DCT features that are transform-based features leveraged signal processing techniques to extract complementary information. Discrete Cosine Transform (DCT) coefficients provided compact frequency-domain representations, with the first five coefficients capturing the most energetically significant spectral components. This approach enabled efficient dimensionality reduction while preserving essential shape information through energy compaction properties. The DCT features proved particularly valuable for identifying systematic variations in spectral shapes corresponding to different adulteration concentrations, offering noise-robust characterization that complemented the statistical features.

Third, normalized shape features provided intensity-invariant morphological descriptors

through min-max normalization and cumulative distribution analysis. Quartile position features identified critical wavelength thresholds where 25%, 50%, and 75% of spectral energy accumulated, characterizing energy distribution patterns across the spectrum. These were augmented by normalized area integration and spectral entropy measurements that quantified the organizational complexity and predictability of spectral signatures.

Together, these three feature categories created a comprehensive multi-perspective feature space capturing 38 statistical, five frequency-domain, and five morphological characteristics essential for detecting subtle adulteration patterns.

Traditional Classifiers

Four traditional classifiers were applied for classification.

- **Support Vector Machine (SVM)**: The Support Vector Machine (SVM) model was implemented using a one-vs-all strategy for multi-class classification. A radial basis function (RBF) kernel was selected to handle potential non-linear decision boundaries in the feature space. The hyperparameters were carefully tuned, with the regularization parameter C set to 1 to balance margin maximization and classification error, and the kernel scale configured indirectly via gamma (set to 0.01), controlling the influence of individual training examples. This configuration aimed to maximize generalization performance while maintaining computational efficiency.
- **Random Forest (RF)**: The Random Forest classifier was implemented to perform the binary classification task. This ensemble method constructs a multitude of decision trees during training and outputs the mode of their predictions for classification. The model was configured with 100 trees, utilizing bootstrap aggregation and Gini's impurity criterion for splitting. Each tree was grown to maximum depth by setting the minimum leaf size to the default value of 1, allowing nodes to split until purity was achieved. Feature randomness was introduced by selecting a random subset of features—equal to the square root of the total number of predictors—for each split, further decorrelating the trees and enhancing model robustness. The combination of these parameters ensured a strong ensemble capable of high generalization performance, as validated on the independent test set.
- **Gradient Boosting (XGBoost)**: The Gradient Boosting model was implemented using the Adaptive Boosting algorithm. This ensemble method operates sequentially, constructing 100 weak learners where each new learner is focused on correcting the errors made by the previous ones in the ensemble. The algorithm automatically induced decision trees as base learners, which were grown using a standard classification tree template. Unlike Random Forest, which builds trees independently, this method combines them additively to create a strong classifier. By iteratively adjusting the weights of misclassified instances, the model minimized the overall multi-class classification error, enhancing predictive performance through a staged and corrective learning process.
- **K-Nearest Neighbor (KNN):** The KNN classifier was implemented with k set to 5, utilizing a straightforward yet effective instance-based learning approach. This non-parametric method classifies each new data point by examining the five closest neighbors in the feature space according to a chosen distance metric, typically Euclidean distance, and assigning the most frequent class among these neighbors. Unlike model-based algorithms, KNN operates without prior training, relying on the entire labeled dataset at classification time; therefore, classification decisions are made based on local data structure. Although the choice of k critically influences performance, k=5 provides a balance between sensitivity to noise and over-smoothing of boundaries. The algorithm's simplicity and adaptability make it well-suited for varied applications, with its accuracy often further enhanced by optimizing parameters such as distance metrics or incorporating feature selection techniques. Despite potentially increased computational demands for large datasets, KNN remains a robust baseline classifier capable of yielding competitive results

across diverse classification tasks through its intuitive neighbor-voting mechanism.

Deep Learning Architectures

Three models are selected for this part: CNN, LSTM, and hybrid CNN-LSTM. For all three deep learning architectures, the models were trained using the Adam optimizer (learning rate = 0.001), categorical cross-entropy loss**,** a batch size of 32, and a maximum of 100 epochs with early stopping (patience = 10) to prevent overfitting. The number of layers and units in each architecture were determined through systematic trial-and-error experimentation on a validation set, as detailed in the respective subsections below.

- **CNN**: A one-dimensional Convolutional Neural Network (1D-CNN) was designed to learn hierarchical feature representations directly from the raw input sequences. The network begins with an input layer accepting 1D data of a specified length. The architecture consists of three convolutional blocks, each comprising a 1D convolution with progressively smaller kernel sizes (11, 7, 5) and an increasing number of filters (32, 64, 128), followed by batch normalization, a ReLU activation function, and max-pooling for dimensionality reduction. Aggressive pooling and strategic dropout layers (rates of 0.3 to 0.5) were incorporated after convolutional layers to prevent overfitting and enhance generalization. The final feature maps are summarized via a global average pooling layer before being passed through two fully connected layers for classification. The network culminates in a softmax layer to output class probabilities. The CNN was trained using the Adam optimizer (learning rate = 0.001), categorical cross-entropy loss, a batch size of 32, and a maximum of 100 epochs with early stopping (patience = 10). The three-layer architecture was selected based on systematic trial-and-error (testing 1–5 layers), as three layers yielded the best validation accuracy with minimal overfitting. This deep architecture allows the model to automatically extract relevant temporal features at varying timescales, from local patterns to more global contexts.

- **LSTM**: A Long Short-Term Memory (LSTM) recurrent neural network was implemented to model the sequential dependencies within the spectral data. The network was designed to process each sample as a univariate time series of 993 features across a single timestep. The architecture comprised two LSTM layers: a first layer with 128 hidden units returning a full sequence output, followed by a second layer with 64 hidden units returning only the final output to capture long-range contextual information. Each LSTM layer was succeeded by batch normalization and a ReLU activation function to stabilize and accelerate training, with dropout layers (rates of 0.3 and 0.4) inserted to mitigate overfitting. The extracted temporal features were then passed through a fully connected layer of 32 units, another dropout layer (rate=0.5), and a final classification layer with a softmax activation function to output class probabilities. This architecture was specifically chosen to leverage the LSTM's ability to learn complex, long-range patterns within the spectral sequences, providing a complementary approach to the feature-learning strategy of the CNN.

- **CNN-LSTM**: A hybrid Convolutional Neural Network-Long Short-Term Memory (CNN-LSTM) architecture was developed to synergistically combine the strengths of both feature extraction and sequential modeling. The model begins with a series of one-dimensional convolutional blocks designed to extract hierarchical local features from the raw spectral data. Each convolutional layer, utilizing progressively smaller kernel sizes (11, 7, 5) and an increasing number of filters (32, 64, 128), is followed by batch normalization, ReLU activation, and max-pooling operations to enhance feature learning and provide translational invariance. The extracted feature maps are then condensed via global average pooling and reshaped into a sequential format. This processed feature sequence is fed into an LSTM layer with 64 hidden units, which models the temporal dependencies and contextual relationships between the high-level features learned by the CNN. The final stages consist of

fully connected layers that integrate these spatially and temporally enriched representations for classification. This hybrid approach effectively captures both the local spectral patterns through convolutional operations and the global sequential dependencies through recurrent connections, providing a comprehensive framework for analyzing the complex structure of spectroscopic data.

Experimental Setting

The dataset was split into training, validation, and testing sets using an 80:10:10 ratio. Hyperparameter optimization was performed exclusively on the validation set: grid search was applied for traditional machine learning classifiers, while random search combined with early stopping was used for deep learning models. The final test set remained completely unseen until the final evaluation. Model performance was assessed using accuracy, precision, recall, and F1-score.

The experiments were conducted using MATLAB 2022 and Python 3.12 on a desktop workstation equipped with an NVIDIA GeForce RTX 4060 Ti GPU (16 GB memory).

Prior to the main experiments, preliminary investigations were conducted to determine appropriate input representations for each model family. These trials evaluated traditional classifiers (RF, GB, SVM, k-NN) using both raw spectral vectors and engineered feature sets. Results consistently showed that traditional classifiers underperformed on raw spectra due to the high dimensionality (hundreds of bands), strong collinearity between adjacent bands, and limited capacity to model sequential spectral patterns. Conversely, engineered features—statistical descriptors, DCT coefficients, and shape features—significantly improved their performance by condensing relevant information into a lower-dimensional, less redundant space.

Deep learning models (CNN, LSTM, CNN-LSTM), however, were designed to accept raw spectral sequences directly, as their architectures are inherently capable of learning temporal/spectral dependencies without manual feature engineering. Therefore, the final experimental framework intentionally uses engineered features for traditional classifiers and raw spectral data for deep learning models. This design leverages the respective strengths of each approach and reflects a practical scenario where simpler models benefit from preprocessing while advanced architectures do not.

RESULTS AND DISCUSSION

Spectral Characteristics Analysis

The mean spectra (Figure 4b) revealed subtle but consistent shape differences in the 680-700nm region across adulteration levels. While no distinct peaks or valleys were observed, the curvature variations provided sufficient discriminatory information. The 5% adulteration class showed the most challenging differentiation from pure sumac.

Traditional Machine Learning Performance

In our comprehensive evaluation of various traditional machine learning algorithms for detecting red sumac adulteration with barberry, we observed notable performance differences across classifiers and feature types (Table 1). RF emerged as the superior traditional classifier with an overall accuracy of 91.11% when utilizing the complete feature set. This finding aligns with previous research highlighting RF's effectiveness in hyperspectral image classification tasks (Su & Sun, 2018). RF has shown robust performance across various hyperspectral applications due to its ability to handle high-dimensional spectral data without overfitting and its inherent feature importance ranking capabilities (Jia et al., 2021; Lu et al., 2020). These characteristics make it particularly suitable for food authentication applications, where distinguishing between subtle spectral differences is critical.

When analyzing performance based on individual feature types, both RF and GB demonstrated excellent performance with statistical features (89.94% and 89.40% accuracy, respectively), significantly outperforming SVM (81.05%) and KNN (78.48%). For DCT features, KNN performed surprisingly well (88.76%), closely followed by RF (88.22%) and GB

(88.01%), while SVM lagged behind (81.91%). With shape features, GB, SVM, and RF all outperformed KNN, suggesting shape characteristics require more complex decision boundaries than what KNN can effectively model.

The confusion matrix of the RF model (as the best traditional machine learning model), illustrated in Figure 5, reveals that most misclassifications occurred between adjacent classes—particularly between Class 1 and Class 2, which correspond to pure sumac and 5% adulteration, respectively. This indicates that the model occasionally struggled to distinguish between pure and minimally adulterated samples, likely due to their highly similar spectral or compositional characteristics. Nevertheless, the RF model demonstrated strong discriminative ability for higher levels of adulteration, showing high confidence in correctly classifying pure sumac and samples with 20% adulteration or more. These results suggest that while the model may exhibit some uncertainty at the boundary between very similar classes, its overall classification performance remains robust for practical detection of adulteration

Table 1: Traditional classifier performance metrics

Method	Features	Accuracy (%)	Precision (%)	Recall (%)	F1-score (%)
SVM	Statistical features	81.05	81.28	81.22	81.22
	DCT features	81.91	82.42	82.09	82.11
	shape features	79.55	79.52	79.60	79.50
	All feature	86.30	86.33	86.39	86.34
RF	Statistical features	89.94	89.99	90.02	89.99
	DCT features	88.22	88.31	88.26	88.27
	shape features	78.16	77.96	78.19	78.06
	All feature	91.11	91.13	91.16	91.14
GB	Statistical features	89.40	89.47	89.44	89.40
	DCT features	88.01	88.15	88.16	88.11
	shape features	79.98	79.89	80.01	79.89
	All feature	90.36	90.55	90.40	90.38
KNN	Statistical features	78.48	78.77	78.65	78.67
	DCT features	88.76	88.78	88.81	88.79
	shape features	75.70	75.70	75.72	75.67
	All feature	82.23	82.29	82.37	82.30

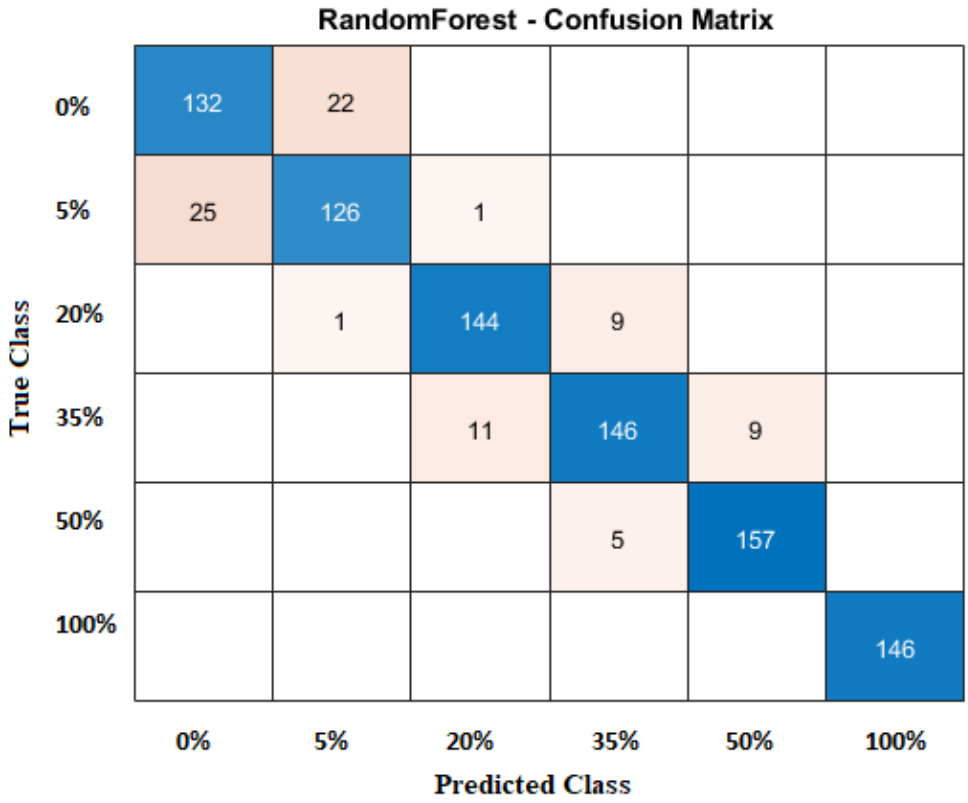

Figure 5. Confusion matrix of RF classifier on the test set. The class labels correspond to: 0% (pure sumac), 5% (5% adulterated sumac), 20% (20% adulterated sumac), 35% (35% adulterated sumac), 50% (50% adulterated sumac), and 100% (pure barberry).

Deep Learning Architecture Performance

Our investigation into deep learning architectures yielded intriguing results, shown in Table 2. LSTM network demonstrated exceptional performance with accuracy exceeding 96%, substantially outperforming CNN at 88.44% and the hybrid CNN-LSTM architecture at 91%. The superior performance of LSTM can be attributed to its inherent ability to capture sequential dependencies in spectral data. As observed in previous hyperspectral studies, the sequential nature of spectral reflectance patterns contains critical discriminative information (Kamruzzaman, 2016). Mou et al. demonstrated that recurrent neural networks are particularly effective for hyperspectral image classification precisely because they preserve and leverage this sequential information. Our findings strongly support this conclusion (Mou et al., 2017).

Interestingly, the CNN model (88.44% accuracy) performed worse than our best traditional classifier, RF (91.11%). This unexpected result suggests that for our specific adulteration detection task, manually engineered features combined with RF can outperform automatic feature extraction via CNN. This finding challenges the common assumption that deep learning always outperforms traditional approaches (Chen et al., 2015; Signoroni et al., 2019) and highlights the importance of selecting appropriate architectures for specific hyperspectral classification tasks.

The hybrid CNN-LSTM model (91% accuracy) performed better than CNN alone but still fell short of the pure LSTM architecture. This suggests that the sequential modeling capability of LSTM remains the dominant factor in this classification task. Training progress of LSTM as the best our model is shown in Figure 6.

Finally, the performance of the LSTM model on the test set is illustrated as a confusion matrix in Figure 7. Compared with the Random Forest (RF) confusion matrix shown in Figure 5, the

LSTM demonstrates improved capability in distinguishing between adjacent classes, indicating its enhanced feature learning and temporal pattern recognition. However, the primary challenge remains in differentiating between pure sumac (Class 1) and the 5% adulterated samples (Class 2). This persistent confusion may be attributed to the low spatial resolution of the used HSI that could limit the model's ability to capture subtle variations.

Table 2: Performance metrics of deep learning architectures

Method	Accuracy (%)	Precision (%)	Recall (%)	F1-score (%)
LSTM	**96.79**	**96.81**	**96.84**	**96.81**
CNN	88.44	88.90	88.50	88.38
CNN_LSTM	91.33	91.44	91.46	91.38

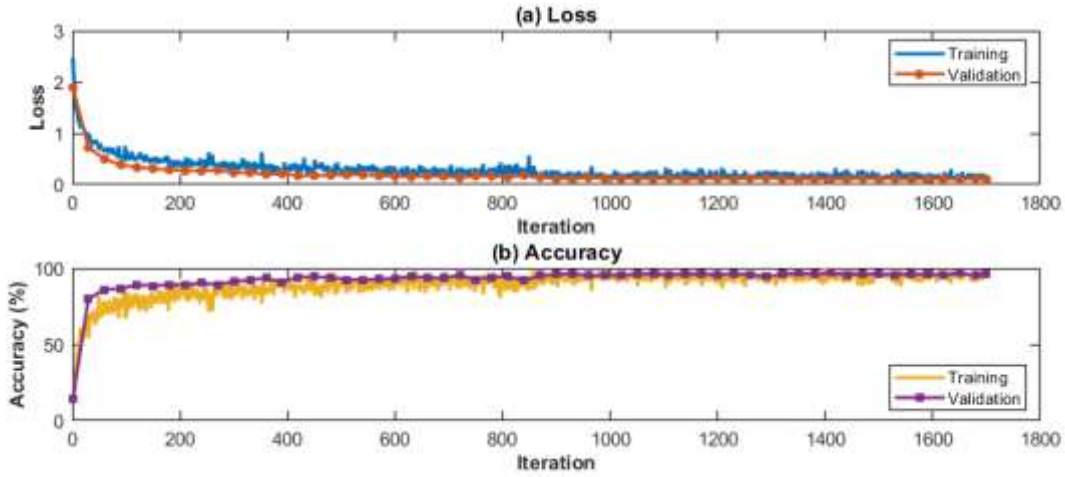

Figure 6. Training progress of LSTM as the best model

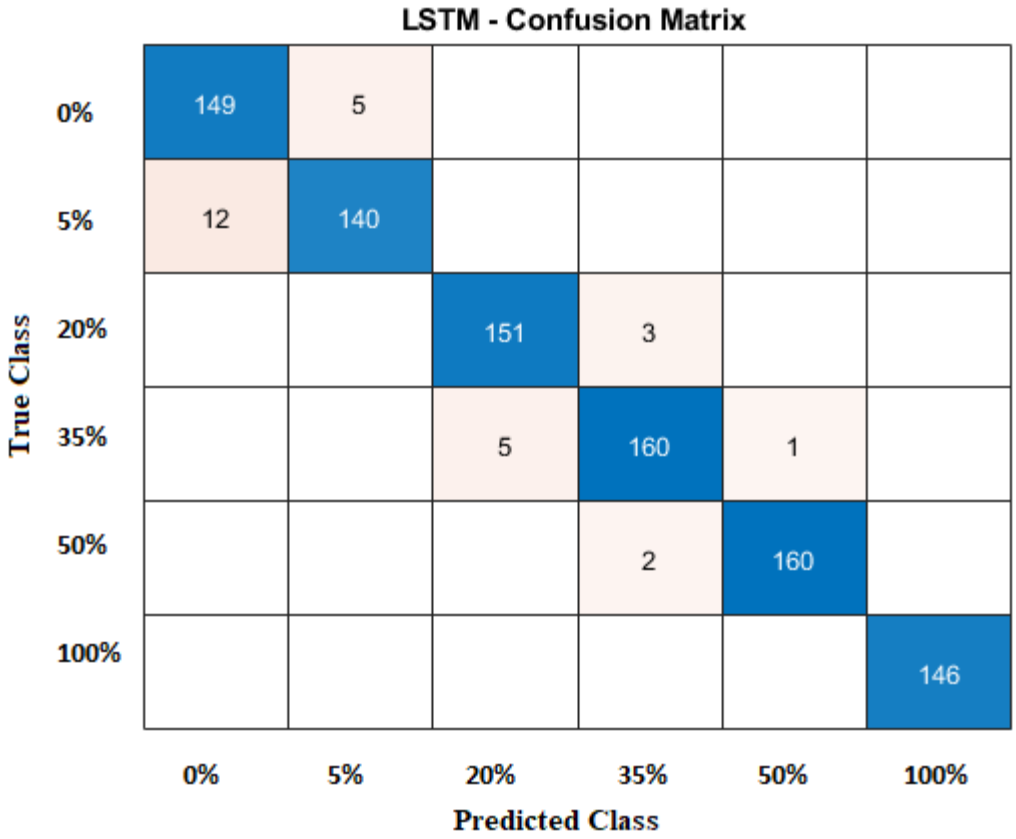

Figure 7. Confusion matrix of LSTM classifier on the test set. The class labels correspond to: 0% = pure sumac, 5% = 5% adulterated sumac, 20% = 20% adulterated sumac, 35% = 35% adulterated sumac, 50% = 50% adulterated sumac, 100% = pure barberry.

Spectral Down Sampling Analysis

To address implementation complexity concerns with LSTM, we conducted a comprehensive down sampling analysis. The downsampling was performed using uniform band decimation, resulting in a reduced set of 33 representative spectral bands. Table 3 demonstrates that even with aggressive down sampling (factor of 30), the LSTM model maintained an impressive 93.9% accuracy. This remarkable robustness to down sampling indicates that the critical spectral signature patterns for red sumac adulteration detection exist at relatively coarse spectral resolutions.

This finding has significant practical implications, as it suggests that lower-cost hyperspectral systems with fewer spectral bands could potentially achieve similar detection performance. Similar spectral redundancy has been observed in previous food adulteration studies (Ahmed, 2024; Aqeel et al., 2024; Fan et al., 2022), where researchers found that carefully selected wavelength bands could maintain classification performance while reducing computational complexity.

The down sampling results also reinforce our conclusion regarding the importance of sequential information in spectral signatures. Even with substantially fewer data points, the LSTM's ability to model the sequence of spectral reflectance values preserved the essential discriminative information. This observation aligns with recent research in food quality assessment using hyperspectral imaging, where sequence-based methods have shown promising results in adulteration detection (Gul et al., 2024; Jiang et al., 2023).

Overall, our findings suggest that while high-resolution spectral data provides the best performance, practical implementations could

achieve an excellent balance between accuracy and computational efficiency through strategic spectral down sampling combined with sequence-based learning approaches.

Table 3: Effect of down sampling of wavelength for LSTM

Down sampling factor	Spectral resolution (nm)	Accuracy (%)	Precision (%)	Recall (%)	F1-score (%)
2	1.1	96.36	96.49	96.40	96.36
4	2.2	96.68	96.71	96.74	96.70
8	4.4	96.04	96.05	96.06	96.04
10	5.5	96.36	96.42	96.37	96.36
20	8.8	95.82	95.83	95.83	95.83
30	16.6	93.90	94.14	93.89	93.87

Practical Implications for Adulteration Detection Systems

The results presented above demonstrate that both traditional machine learning and deep learning approaches can effectively detect barberry adulteration in red sumac using hyperspectral imaging. Among the evaluated methods, the LSTM architecture achieved the highest classification accuracy (96.84%), outperforming CNN-based models and traditional classifiers such as RF (91.11%).

In hyperspectral imaging, wavelengths are acquired in a monotonic sequence (e.g., from visible to near-infrared, 400–950 nm). This ordering is not arbitrary; it reflects the continuous physical decrease of photon energy with increasing wavelength. Consequently, adjacent spectral bands are correlated, and spectral signatures exhibit gradual, structured variations arising from specific molecular absorption features (e.g., O–H, C–H, N–H bonds). This sequential structure makes spectral data conceptually analogous to a time series, where the "sequence position" is wavelength. An LSTM is designed to capture long- and short-range dependencies in sequential data by learning, via its gating mechanisms, which information from previous steps to retain or forget. In the context of adulteration detection, subtle spectral changes caused by mixing barberry into sumac may manifest as local distortions or shifts that extend across several contiguous wavelength bands. An LSTM can model these spectral dependencies more naturally than a standard 1D-CNN, which primarily learns local patterns within a fixed kernel window and lacks an inherent memory of prior spectral positions across long ranges (a 1D-CNN can increase its receptive field by stacking convolutional layers, but it does not explicitly model sequential context).

The comparative analysis across different classifiers and architectures offers valuable insights for developing practical red sumac adulteration detection systems. While LSTM provides the highest accuracy, its implementation complexity must be considered. The down sampling analysis demonstrates that a simplified LSTM model with reduced spectral resolution offers an excellent compromise between performance and implementation feasibility.

The finding that approximately 93.9% of the original classification accuracy is retained after a 30× spectral reduction highlights significant potential for practical, cost-effective implementation. Full-range visible and near-infrared (VNIR) hyperspectral imaging (HSI) systems, such as pushbroom cameras capturing hundreds of contiguous bands (e.g., 993 bands between 400–950 nm), require complex optical components and are highly expensive. Commercial systems of this specification typically range from $50,000 to $70,000 USD, depending on the lens and integration hardware.

In stark contrast, transitioning to a targeted multispectral sensing system utilizing the 33 selected downsampled bands drastically reduces hardware requirements. A customized multispectral setup can be constructed using a standard industrial monochrome CMOS camera (approximately $500–$1,000 USD), a motorized

filter wheel (approximately $1,000–$1,500 USD), and 33 specific optical bandpass filters corresponding to the downsampled wavelengths (approximately $100–$150 per filter, totaling ~$3,300–$5,000 USD). Consequently, the estimated cost for such a 33-band multispectral system ranges from $5,000 to $8,000 USD. This represents an approximate 85–90% reduction in initial hardware costs compared to a full hyperspectral system. Given that this substantial cost reduction yields only a marginal 6.1% drop in classification accuracy, the proposed spectral downsampling strategy provides a highly viable pathway for deploying scalable, affordable multispectral sensors in large-scale food safety assessment applications.

These findings contribute to the growing body of research on food adulteration detection using hyperspectral imaging and machine learning (Aqeel et al., 2024; Kamruzzaman, 2016; Temiz & Ulaş, 2021) Similar to our results, recent studies on detecting adulterants in oils (Aqeel et al., 2024), and honey (Ahmed, 2024)have demonstrated the effectiveness of both traditional machine learning and deep learning approaches when combined with hyperspectral imaging.

Our work particularly highlights the importance of sequential spectral information, which aligns with findings from recent studies employing recurrent neural networks for food quality assessment (Gul et al., 2024). The successful application of LSTM to our red sumac adulteration detection problem reinforces the potential of sequence-based deep learning approaches for similar food authentication challenges.

Despite the promising results, several limitations should be acknowledged. First, the dataset, while carefully controlled, was acquired under laboratory conditions with uniform illumination and sample presentation. Real-world scenarios involve variable lighting, sample heterogeneity, and different grinding or drying processes, which may affect model performance. Second, this study focused exclusively on barberry as the adulterant; other potential adulterants (e.g., pomegranate seeds, cheap plant powders) were not tested. Third, the sample size (150 per class) is moderate; larger and more diverse sample sets would further validate generalization. Future work should include field-deployable multispectral prototype testing, evaluation on other sumac varieties and adulterants, and integration of the LSTM model into a real-time sorting or quality control system. Additionally, explainable AI techniques (e.g., SHAP or LIME) could be employed to interpret the spectral features most critical for LSTM decisions, increasing trust for regulatory applications.

CONCLUSIONS

This study demonstrates a comprehensive machine learning framework for detecting red sumac adulteration with barberry using hyperspectral imaging. Among traditional classifiers, Random Forest with engineered features achieved the highest practical utility (91.11% accuracy) with computational efficiency suitable for industrial deployment, while deep learning investigations revealed that LSTM networks, leveraging sequential spectral information, outperformed all other methods (96%+ accuracy). Notably, even under 30× spectral downsampling—reducing spectral resolution to 16.6 nm—LSTM maintained 93.9% accuracy, highlighting the potential for cost-effective implementations with multispectral image sensors. Future work will focus on real-time field deployment using low-cost multispectral sensors, and expansion to other spice adulterants. The proposed framework offers a non-destructive, rapid quality control solution that balances classification accuracy with hardware complexity, contributing to broader efforts in food authenticity and safety assurance.

ACKNOWLEDGEMENTS

The authors acknowledge the assistance of DeepSeek, OpenAI’s GPT-4o, and Qwen AI in the language refinement of this manuscript.

AUTHOR CONTRIBUTION

A. Basiri prepared the samples. F. Rahmani acquired the hyperspectral images. S. Shojaeilangari developed and implemented the algorithms. All authors contributed to the writing, editing, and proofreading of the manuscript. E. K. Farahani, S. Shojaeilangari, and A. Basiri supervised the data collection and analysis of the project.

FUNDING

No funding was received to assist with the preparation of this manuscript.

DATA AVAILABILITY

The dataset generated and analyzed during the current study will be made available from the corresponding author upon reasonable request.

DECLARATION OF COMPETING INTEREST

The authors have no competing interests to declare that are relevant to the content of this article.

REFERENCES

Ahmad, M., Shabbir, S., Roy, S. K., Hong, D., Wu, X., Yao, J., Khan, A. M., Mazzara, M., Distefano, S., & Chanussot, J. (2021). Hyperspectral image classification—Traditional to deep models: A survey for future prospects. *IEEE journal of selected topics in applied earth observations and remote sensing*, *15*, 968–999. https://doi.org/10.1109/JSTARS.2021.3133021

Ahmed, E. (2024). Detection of honey adulteration using machine learning. *PLOS digital health*, *3*(6), e0000536. https://doi.org/10.1371/journal.pdig.0000536

Aqeel, M., Sohaib, A., Iqbal, M., Rehman, H. U., & Rustam, F. (2024). Hyperspectral identification of oil adulteration using machine learning techniques. *Current Research in Food Science*, *8*, 100773. https://doi.org/10.1016/j.crfs.2024.100773

Chen, Y., Zhao, X., & Jia, X. (2015). Spectral–spatial classification of hyperspectral data based on deep belief network. *IEEE journal of selected topics in applied earth observations and remote sensing*, *8*(6), 2381–2392. https://doi.org/10.1109/JSTARS.2015.2388577

Fan, B., Zhu, R., He, D., Wang, S., Cui, X., & Yao, X. (2022). Evaluation of mutton adulteration under the effect of mutton flavour essence using hyperspectral imaging combined with machine learning and sparrow search algorithm. *Foods*, *11*(15), 2278. https://doi.org/10.3390/foods11152278

Ferrari, V., Calvini, R., Menozzi, C., Ulrici, A., Bragolusi, M., Piro, R., Tata, A., Suman, M., & Foca, G. (2024). Addressing adulteration challenges of dried oregano leaves by NIR HyperSpectral Imaging. *Chemometrics and Intelligent Laboratory Systems*, *249*, 105133. https://doi.org/10.1016/j.chemolab.2024.105133

Fu, H., Zhang, A., Sun, G., Ren, J., Jia, X., Pan, Z., & Ma, H. (2022). A novel band selection and spatial noise reduction method for hyperspectral image classification. *IEEE transactions on geoscience and remote sensing*, *60*, 1–13. https://doi.org/10.1109/TGRS.2022.3189015

Galvin-King, P., Haughey, S. A., & Elliott, C. T. (2018). Herb and spice fraud; the drivers, challenges and detection. *Food Control*, *88*, 85–97. https://doi.org/10.1016/j.foodcont.2017.12.031

Grivetti, L. E. (2016). Herbs, spices, and flavoring agents: Part 1: Old world contributions. *Nutrition Today*, *51*(3), 139–150. https://doi.org/10.1097/NT.0000000000000149

Gul, N., Muzaffar, K., Shah, S. Z. A., Assad, A., Makroo, H. A., & Dar, B. (2024). Deep learning hyperspectral imaging: a rapid and reliable alternative to conventional techniques in the testing of food quality and safety. *Quality Assurance and Safety of Crops & Foods*, *16*(1), 78–97. https://doi.org/10.15586/qas.v16i1.1392

Jia, S., Jiang, S., Lin, Z., Li, N., Xu, M., & Yu, S. (2021). A survey: Deep learning for hyperspectral image classification with few labeled samples. *Neurocomputing*, *448*, 179–204. https://doi.org/10.1016/j.neucom.2021.03.035

Jiang, Z., Lv, A., Zhong, L., Yang, J., Xu, X., Li, Y., Liu, Y., Fan, Q., Shao, Q., & Zhang, A. (2023). Rapid prediction of adulteration content in Atractylodis rhizoma based on data and image

features fusions from near-infrared spectroscopy and hyperspectral imaging techniques. *Foods*, *12*(15), 2904. https://doi.org/10.3390/foods12152904

Johnson, N. A. N., Adade, S. Y.-S. S., Ekumah, J.-N., Kwadzokpui, B. A., Xu, J., Xu, Y., & Chen, Q. (2025). A comprehensive review of analytical techniques for spice quality and safety assessment in the modern food industry. *Critical reviews in food science and nutrition*, *65*(30), 7225–7250. https://doi.org/10.1080/10408398.2025.2462721

Khan, M. H., Saleem, Z., Ahmad, M., Sohaib, A., Ayaz, H., & Mazzara, M. (2020). Hyperspectral imaging for color adulteration detection in red chili. *Applied Sciences*, *10*(17), 5955. https://doi.org/10.3390/app10175955

Kiani, S., van Ruth, S. M., van Raamsdonk, L. W., & Minaei, S. (2019). Hyperspectral imaging as a novel system for the authentication of spices: A nutmeg case study. *Lwt*, *104*, 61–69. https://doi.org/10.1016/j.lwt.2019.01.045

Kishani Farahani, E., & Shojaielangari, S. (2026). Non-Destructive Authentication of Rice Varieties Using Hyperspectral Imaging and Machine Learning. *Biomechanism and Bioenergy Research*, *5*(1), 1–19. https://doi.org/10.22103/bbr.2026.26384.1142

Liu, T., Zhang, W., Xu, H., Yu, J., Sang, T., Wang, Y., & Wang, S. (2025). Non-destructive quantitative detection of lymphatic meat adulterated in beef by hyperspectral imaging combined with interpretable deep learning. *Food Control*, *181*, 111742. https://doi.org/10.1016/j.foodcont.2025.111742

Lu, B., Dao, P. D., Liu, J., He, Y., & Shang, J. (2020). Recent advances of hyperspectral imaging technology and applications in agriculture. *Remote sensing*, *12*(16), 2659. https://doi.org/10.3390/rs12162659

Meng, R., Lv, Z., Yan, J., Chen, G., Zhao, F., Zeng, L., & Xu, B. (2020). Development of spectral disease indices for southern corn rust detection and severity classification. *Remote sensing*, *12*(19), 3233. https://doi.org/10.3390/rs12193233

Mou, L., Ghamisi, P., & Zhu, X. X. (2017). Deep recurrent neural networks for hyperspectral image classification. *IEEE transactions on geoscience and remote sensing*, *55*(7), 3639–3655. https://doi.org/10.1109/TGRS.2016.2636241

Orrillo, I., Cruz-Tirado, J., Cardenas, A., Oruna, M., Carnero, A., Barbin, D. F., & Siche, R. (2019). Hyperspectral imaging as a powerful tool for identification of papaya seeds in black pepper. *Food Control*, *101*, 45–52. https://doi.org/10.1016/j.foodcont.2019.02.036

Sahu, P. K., Purohit, S., Tripathy, S., Mishra, D. P., & Acharya, B. (2023). Current trends in HPLC for quality control of spices. In *High Performance Liquid Chromatography-Recent Advances and Applications*. IntechOpen. https://doi.org/10.5772/intechopen.110897

Savitzky, A., & Golay, M. J. (1964). Smoothing and differentiation of data by simplified least squares procedures. *Analytical chemistry*, *36*(8), 1627–1639. https://doi.org/10.1021/ac60214a047

Schumer, N. G., Ahmed, M. W., Rausch, K., Singh, V., & Kamruzzaman, M. (2025). Chemometric-based approach for economically motivated fraud detection in organic spices via NIR spectroscopy. *Journal of Food Composition and Analysis*, *142*, 107538. https://doi.org/10.1016/j.jfca.2025.107538

Sebaei, A. S., Youssif, M. I., & Ghazi, A. A.-M. (2019). Determination of seven illegal dyes in Egyptian spices by HPLC with gel permeation chromatography clean up. *Journal of Food Composition and Analysis*, *84*, 103304. https://doi.org/10.1016/j.jfca.2019.103304

Sharma, A., & MMR, M. (2022). A HPTLC method for the quantitative determination of Piperine and Capsaicin in Rasam, A South Indian spice soup. *Int J Ayurvedic Med*, *13*(2), 483–486. https://doi.org/10.47552/ijam.v13i2.2548

Shojaeilangari, S., Kishani Farahani, E., & Basiri, A. (2026). Deep Learning-Enabled Hyperspectral Classification of ham. *Innovative Food Technologies*, *13*(3), 281–295. (In Persian) https://doi.org/10.22104/ift.2025.8010.2255

Signoroni, A., Savardi, M., Baronio, A., & Benini, S. (2019). Deep learning meets hyperspectral image analysis: A multidisciplinary review. *Journal of imaging*, *5*(5), 52. https://doi.org/10.3390/jimaging5050052

Su, W. H., & Sun, D. W. (2018). Fourier transform infrared and Raman and hyperspectral imaging techniques for quality determinations of powdery foods: A review. *Comprehensive Reviews in Food Science and Food Safety*, *17*(1), 104–122. https://doi.org/10.1111/1541-4337.12314

Temiz, H. T., & Ulaş, B. (2021). A review of recent studies employing hyperspectral imaging for the determination of food adulteration. *Photochem*, *1*(2), 125–146. https://doi.org/10.3390/photochem1020008